BOUNDARY LAYER TRANSITION, SEPARATION AND FLOW CONTROL ON AIRFOILS AND BODIES IN CFD, WIND-TUNNEL AND IN-FLIGHT STUDIES

POPELKA Lukas* – SIMURDA David* – MATEJKA Milan – SOUCKOVA Natalie***
*** Institute of Thermodynamics, Academy of Sciences of the Czech Republic,**
****Faculty of Mechanical Engineering, Czech Technical University in Prague**

Keywords: *Flow Control, Transition and Turbulence, Wind Tunnel and Flight Testing*

Abstract

Particle Image Velocimetry, smoke-wire, tuft filaments and oil-flow visualization techniques were used for wind-tunnel and in-flight investigation of boundary layer separation, both stall and separation bubbles, related to the low-Reynolds number transition mechanism. Airfoils of three Czech-designed sailplanes and their wing-fuselage interaction were subject to study. Wind-tunnel experiments, in-flight test cases on sailplanes were used, and synthesis with CFD data gained. Effect of passive flow control devices - vortex generators - was surveyed, counter-rotating vortex generators and Zig-zag type turbulators were applied. Separation suppression was reached and consequent drag coefficient reduction of test aircrafts measured in flight. Investigation was further extended by PIV Time-Resolved technique.

1 Introduction

Boundary layer developpent along the airframe is important for any aircraft, taking top importance for sailplanes, since directly related to their performance [1]. Sailplane design, has been almost exclusively linked with applied and primary research. Most of new findings are regularly internationally shared by the OSTIV (Organisation Scientifique et Technique Internationale du Vol à Voile) activities.

2 Geometries subject to study

The primary and applied research was coupled with three Czech designed and manufactured saiplanes, Figs 1 and 2.

VSO10 is the most widely used single-seat sailplane in the Czech Republic. TST10 is a new microlight sailplane with self-launching ability, aimed at leisure flying and club class handicaped competition. HPH304S is a new 18m FAI class racing sailplane, produced also with piston-engine self-launcher or jet-engine sustainer option.

For mutual comparison, the last generation club class sailplane, the HPH304C was added to the research programme, Fig. 1.

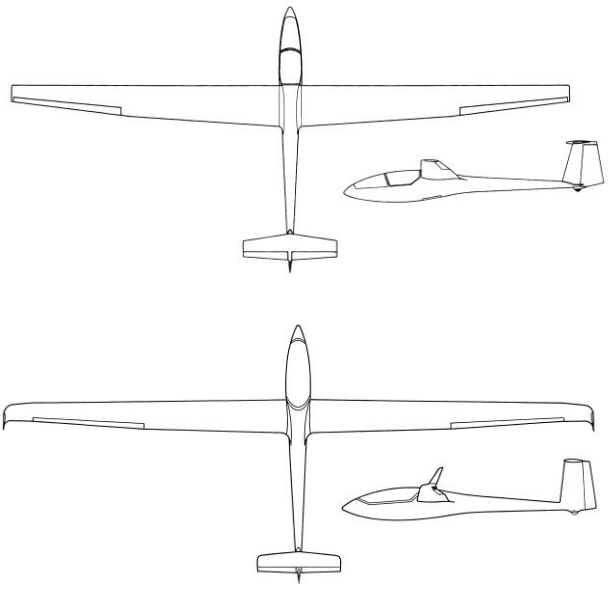

Fig. 1. Club class sailplanes VSO10, HPH304C, both 15m wingspan (from top to bottom)

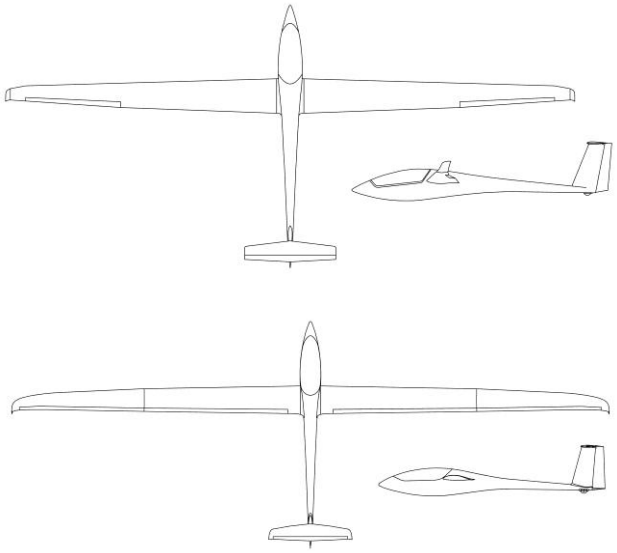

Fig. 2. Self-launching sailplanes TST10 (15m), HPH304S (18m flapped) (from top to bottom)

VSO10 test programme employed an outer wing segment, adopted for wind-tunnel height. The whole section features linear transition from Wortmann FX60-126 to FX61-163 airfoil [2]; considering the tip itself, dominant geometry is the FX60-126 with 25% chord aileron. Enabling mutual comparison, the wingtip with aileron was built in the negative moulds of HPH304C sailplane. For wing-fuselage interaction study, a series sailplane VSO10C call-sign OK-0530 was used.

TST10 research programme was initiated by in-flight measurements on a particular self-launching TST-10a sailplane OK-A631. The fuselage shape followed published coordinates [3] (Model No. 1) and, together with a Wortmann FX66 series wing airfoil [2], created a suitable test case for this interaction investigation, denoted as T10.

The geometry of the computational model was simplified in comparison to the real aircraft - the empennage was omitted and only the inner part of the wing was considered, having a simplified rectangular planform. Also, the small fillet in the junction of the wing and the fuselage was neglected to make easier the preparation of the mesh.

The 1:5 scale wind-tunnel model was based on the previously mentioned geometry for CFD. The span was reduced to fit the height of the test section. The fillets of the real geometry were retained.

HPH304S wing employs a proprietary, company-developed airfoil HPH_x_n2, designed for turbulator on lower side. In-flight testing for optimum flap setting and evaluation of fuselage influence upon the wing was carried out on first prototype, call-sign OK-0111.

3 Analysis methods

Three CFD codes, three wind-tunnels and three test aircraft were used for analysis of flow, with particular details on transition coupled with separation bubble and both laminar and turbulent separation.

3.1 Numerical modelling

For the airfoil analysis, standard tool Xfoil [4] was used. In order to investigate the properties of the whole wing, XFLR5 [5] software was used.

Commercial code Fluent 6.3 was used for 3D numerical simulation. Concerning the computational domain for finite volume calculation, the applied types of boundary conditions can be seen in Fig. 3.

In order to ensure accurate results and to keep computational costs as low as possible, a hexahedral grid was used for meshing of the computational domain, Fig. 4. The mesh was refined at walls. Due to problems with geometry, however, the laminar sub-layer was not resolved everywhere in the domain. The maximum value of y^+ was 17.

Flow properties at the inlet were characterized by prescribed inlet velocity v and the inlet turbulence intensity Tu was 0.2%. The second order accuracy scheme was used for discretization of governing equations. Turbulent flow was modelled using realizable k-ε model of turbulence [6], which performs well in flows involving rotation, boundary layers under strong adverse pressure gradients, separation and recirculation. Spalart-Allmaras and sst k-ω turbulence models [7], [8] were assessed as well. The effect on the analysed results, however, was insignificant. Near-wall

flow was modelled using a combination of a two-layer model and wall functions.

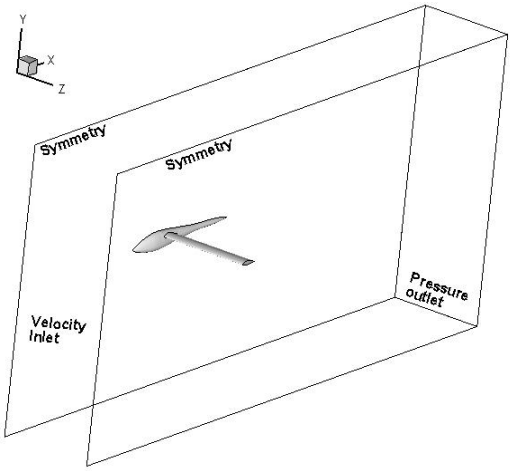

Fig. 3. Scheme of the computational domain with boundary condition types

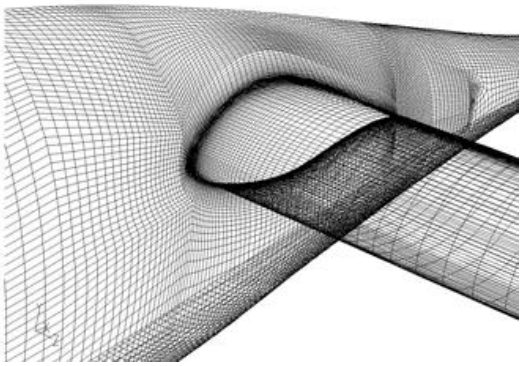

Fig. 4. Mesh of the computational domain

3.2 Wind-tunnel measurement

The closed-circuit, open test section, general purpose wind-tunnel of the Faculty of Mechanical Engineering, Czech Technical University in Prague was used for smoke-wire, oil flow and infrared camera visualization. Airfoil model with circular end plates was located horizontally, Fig. 5. Typical Reynolds number was Re = 3e5 and inlet turbulence intensity *Tu* = 2.2%.

Blow-down rig with outlet cross-section 250x250mm^2 of the Institute of Thermomechanics Academy of Sciences CR, Fig. 6, was employed for Time-Resolved PIV measurement at Re = 1e5 and *Tu* = 0.5%.

The closed-circuit, closed test section, research wind-tunnel of the Institute of Thermomechanics Academy of Sciences CR was used for all remaining test programme. A test section of dimensions 865 x 485 x 900mm was designed for airfoil and wing-body investigations [9]. Circular end plates provide an attachment for both types of models.

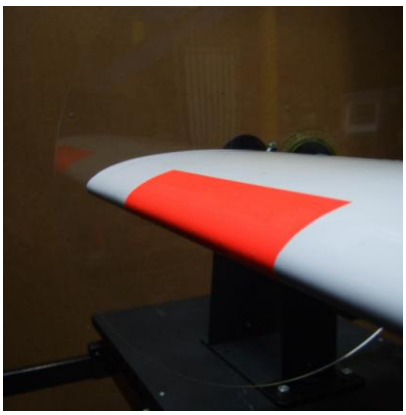

Fig. 5. VSO10 wing segment with end plates, simulated strip of roughness due to insect, 750x550mm^2 wind-tunnel CTU in Prague

Fig. 6. Blow-down rig 250x250mm^2 IT AS CR, TR PIV setup

Fig. 7. T10 test case geometry in the 865x485mm^2 wind-tunnel IT AS CR

The turntables are 500 mm in diameter and are flush with the wind-tunnel walls. They are electrically driven to enable angle of attack changes for the model. The airfoil was mounted so the center of rotation of the circular plates was at 40% of the model chord. The same fraction is preserved for the body model, Fig. 7, with respect to wing chord. The air gaps at the tunnel walls were sealed by labyrinth packing.

Typical Reynolds number was Re = 5e5, inlet turbulence intensity *Tu* through whole range of velocities was 0.2%.

3.3 In-flight measurement

Standard pressure instruments and GPS-based technologies were used for data acquisition. The altimeter and airspeed indicator were connected to factory-designed static ports. A thermocouple was placed outside the canopy frame to measure the flow temperature. GNSS Flight Recorders were used to acquire GPS signals. The recorded flight track was post-processed and the evaluated flight speed and sink rate were reduced to the International Standard Atmosphere. Calibration of the sailplane pitot-static system was obtained. Measurement of the sailplane speed polar was based on GPS methodology [10] which was further refined. Every measurement programme was started at an altitude of 2000 m AGL or higher. Four individual straight flight sequences were used for each airspeed. Flight tracks of 300 m altitude-loss in each sequence were recorded.

Oil flow visualisations at several positions along wingspan were performed on all three sailplanes. Oil was applied on the surface prior to take-off and a flight of 10 minutes duration was carried out. The airspeed was held constant during the whole flight, typically V = 100 km/h IAS, even during the climb and approach to landing.

An array of tufts was applied to the wing root area of VSO10 and TST10a. Video recordings by a cameras located on the tail-boom or on the fuselage top were acquired. To cover the common competition range, airspeeds *V* ranging from 85 to 160 km/h IAS were selected.

An integrating rake was designed, Fig. 8 and tested for drag measurement in wind-tunnels. Further on, it was used for in-flight measurement, fixed to the flaperon of the HPH304S sailplane on wing chord c = 793 mm, Fig. 9.

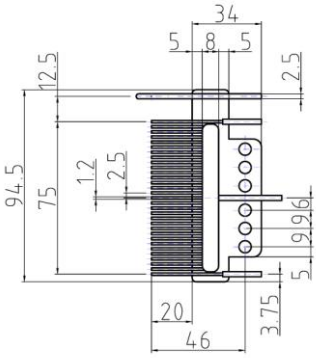

Fig. 8. Integrating pressure rake for in-flight measurement

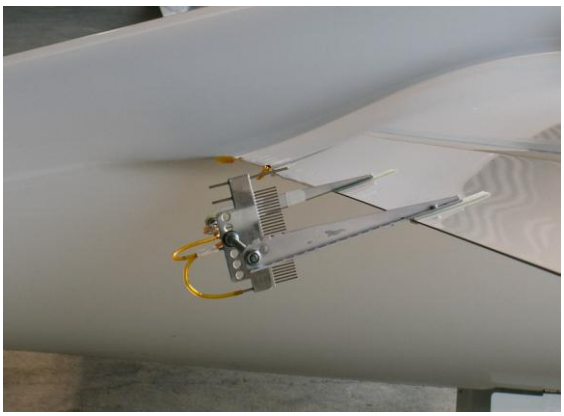

Fig. 9. Installation of pressure rake downstream the wing trailing edge

4 Airfoils, extension to wings

Xfoil and XFLR5 analysis revealed laminar separation on lower side of upward deflected aileron on VSO10 outer wing segment. CFD modelling of forced transition predicted wing roll rate improvement. Lift curve measurement confirmed improvement by Zig-zag type turbulator placed 0.03 x/c upstream aileron hinge, Fig. 10 (lower branch of lift curves).

Beside that, turbulent separation take place on aileron upper surface, while positive deflections. Vane-type rectangular vortex generators of height 3mm were used and substantial improvement of lift properties reached, Fig. 10 (upper branch of lift curves).

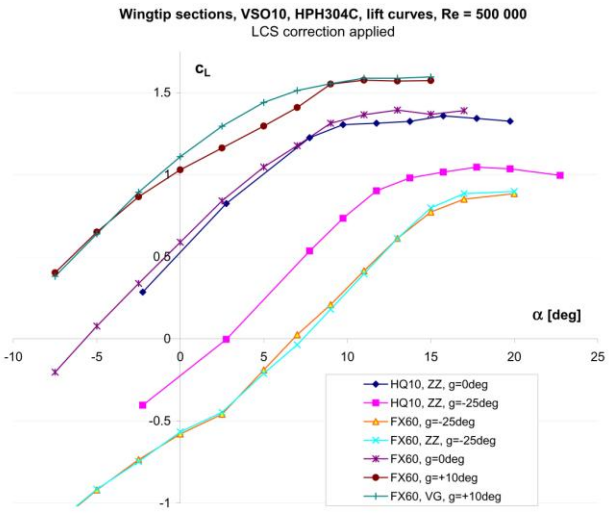

Fig. 10. Comparison of lift curves, Re = 5e5, VSO10 and HPH304C wingtip sections, effect of passive flow control devices

Xfoil and XFLR5 analysis, Fig. 11 showed a potential of performance improvement on TST10 wing by turbulators on lower side. Smoke-wire visualization followed and separation bubble suppression was reached, Fig. 12.

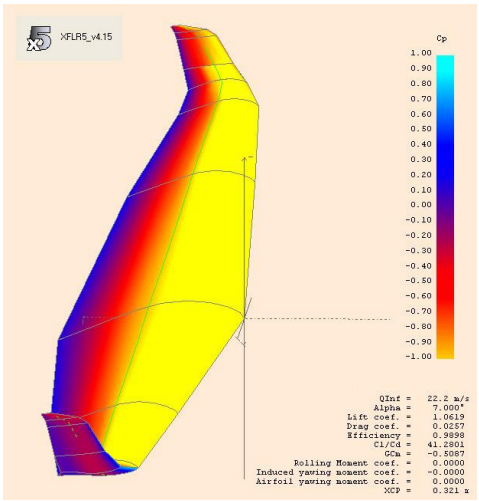

Fig. 11. XFLR5 panel method analysis of TST10a wing, c_L = 1, green line indicates transition

Finally in-flight oil flow visualization was used for identification of separation onset and reattachment, Fig. 13. Zig-zag turbulators applied along wingspan. Speed-polar was measured and served as baseline for further analysis. Gained improvements are similar to successful case of Standard Cirrus sailplane [10] with 10.7% improvement of overall lift-to-drag ratio.

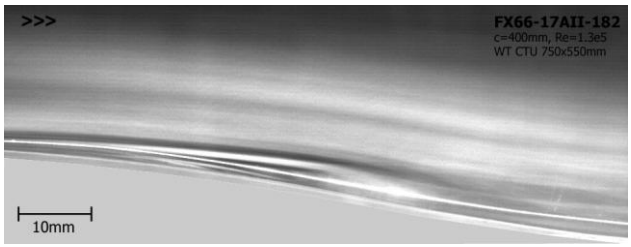

Fig. 12a. FX66-17AII-182 airfoil, smoke-wire visualization, bottom side, Re = 1.3e5, uncontrolled case

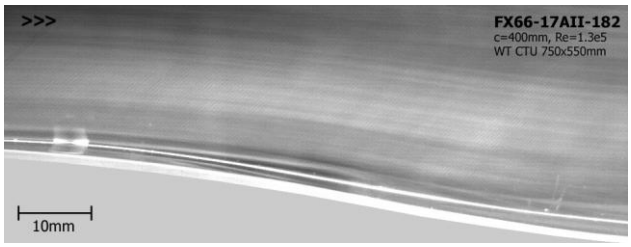

Fig. 12b. FX66-17AII-182 airfoil, smoke-wire visualization, bottom side, Re = 1.3e5, passive-flow control: Zig-zag turbulator, x_{Tb}/c = 0.4

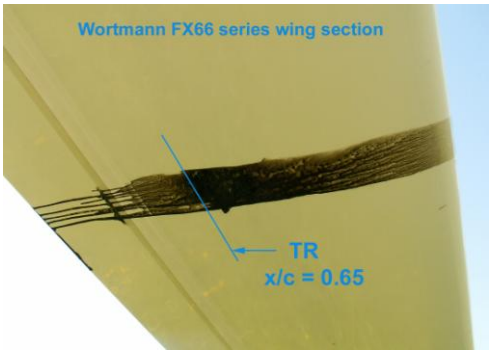

Fig. 13. Oil-flow visualization on lower surface of outer wing segment of TST10a sailplane, in the aileron region. Local chord c = 490 mm, V = 100 km/h IAS. Right to left: laminar boundary layer, separation bubble, turbulent boundary layer; TR – turbulent reattachment line

FX66 family airfoils were further studied by Time-Resolved PIV system. Dantec TR PIV system, with Pegasus Laser 2x10mJ and NanoSense Mk. III camera, served for acquisition of 1635 double-images of 1280x1024 pixels resolution with frequency of 500Hz in each test case – uncontrolled and controlled transition on FX66-S-196V1 airfoil.

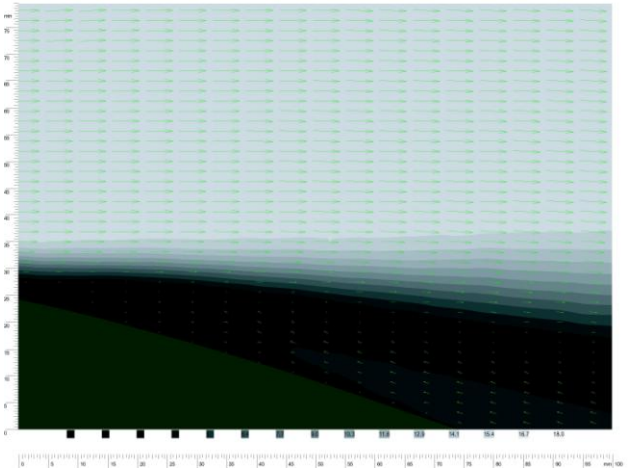

Fig. 14a. FX66-S-196V1 airfoil, TR PIV mean velocity field, top side, Re = 1e5, uncontrolled case

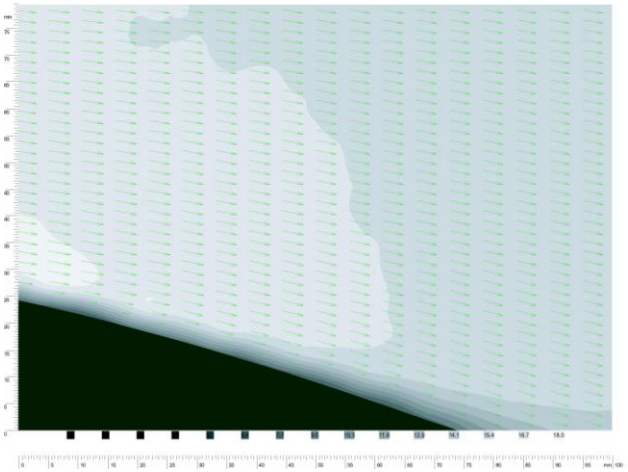

Fig. 14b. FX66-S-196V1 airfoil, TR PIV mean velocity field, top side, Re = 1e5, passive-flow control: Zig-zag turbulator, $x_{Tt}/c = 0.1$

Although mean velocity fields, presented on Fig. 14, namely for the separated boundary layer, correspond well to the established schemes, no such flow behavior is present in instantaneous data. Full potential of Time Resolved technique should be utilised for identifying the unsteady vortex structures.

Possibility of drag coefficient reduction by transition control on the airfoil lower surface, while flap setting for circling, was studied. Surface flow visualization and integrating rake pressure measurement for optimum transition control was carried out on a high-performance sailplane HPH304S. No evidence of separation bubble was found on outer part of the wing and its transition to the winglet. As practical solution, flaperons are equipped in front of their hinge by Zig-zag turbulator. To verify results of calculated optimum location, oil-flow tests were flown on V = 100km/h IAS and integrating rake on V = 85, 100, 120 and 140 km/h IAS. Difference of mean total pressure in the wake p_m and undisturbed total pressure p_∞ , $p_{Rake} = p_\infty - p_m$, was measured by pressure transducer. All data were normalized by the dynamic pressure q:

$$\Pi_{Rake} = p_{Rake} / q \qquad (1)$$

Calculated overall optimum location for turbulator tape and also appropriate flap deflections for given airspeeds were confirmed experimentally. Values of Π_{Rake} for all flap deflections are shown on Fig. 15.

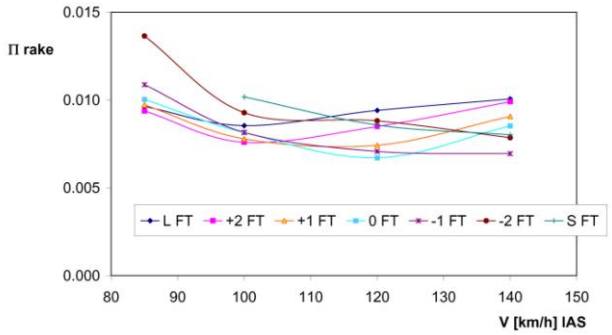

Fig. 15. Normalised integrating rake pressure difference Π_{Rake}. HPH304S sailplane, airfoil chord c = 793 mm, factory installed turbulators (FT configuration)

5 Wing-fuselage interaction

Since some of the effects taking place at the fuselage-wing junction [1] result in generation of vortex structures, these structures needed to be identified in the flowfield. There exist numerous methods of vortex identification. Those methods used in this research are described below.

Mapping of streamlines onto a plane normal to the vortex core

A structure is called a vortex when instantaneous streamlines mapped onto a plane, normal to the vortex core, exhibit roughly a spiral or circular pattern when viewed from

a reference frame moving with the centre of the vortex core [11].

Q-criterion

A vortex exists in locations where rotation dominates over strain. The second invariant of velocity gradient Q is positive in such locations:

$$Q = \frac{1}{2}\left(\Omega_{ij}\Omega_{ij} - S_{ij}S_{ij}\right) \tag{2}$$

$$Q \geq Q_{th} \tag{3}$$

Normalized helicity

The angle between the velocity vector and the vector of vorticity is zero in the vortex core. Normalized helicity is defined as a cosine of this angle:

$$H_n = \frac{w_i \cdot \omega_i}{|w_i| \cdot |\omega_i|} \tag{4}$$

Hence the vortex core is defined as

$$|H_n| = 1. \tag{5}$$

Lower gains of height in dolphin style use of thermals were onset for validation of proper function of wing-fuselage fairing of the VSO10 sailplane. Steep pull-outs from V = 140 km/h IAS till stall were performed. During the whole manoeuvre the flow remained attached, as on Fig. 16a.

Fig. 16a. VSO10C sailplane, wing root tuft visualization, V = 140 km/h IAS, attached flow

The separation revealed only approximately 5 km/h above stall speed, with presence of buffetting, hence desirable properties were confirmed, Fig. 16b.

Fig. 16b. VSO10C sailplane, wing root tuft visualization, V = 70 km/h IAS, bank angle 30deg, stalled flow

CFD analysis procedure, described in section 3.1 and vortex identification, given by equations (2) to (4) was used for T10 test case geometry modelling. Generation of the horseshoe vortex can be seen in Fig. 17. Streamlines in the picture are mapped onto a plane perpendicular to the wing surface in the region of the stagnation point.

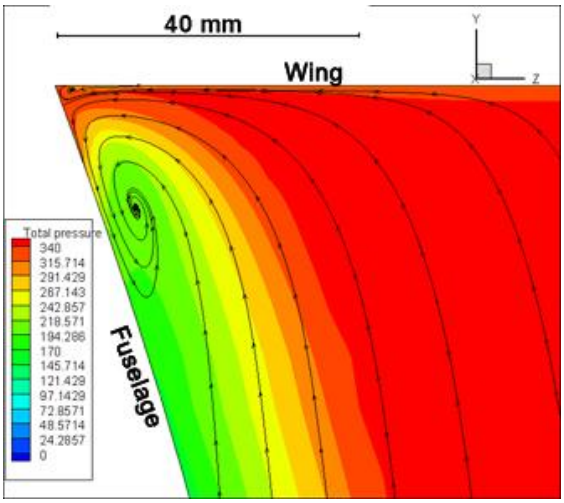

Fig.17. Streamlines mapped onto a plane perpendicular to the wing surface with contours of total (over)pressure

It can be clearly seen how the boundary layer on the fuselage surface separates and forms the vortex. Also, another much smaller contrarotating vortex is observed closer to the leading edge.

Two vortex branches of vortices can be seen in Figure 18. More or less they follow upper and bottom surface of the wing and stretch further downstream.

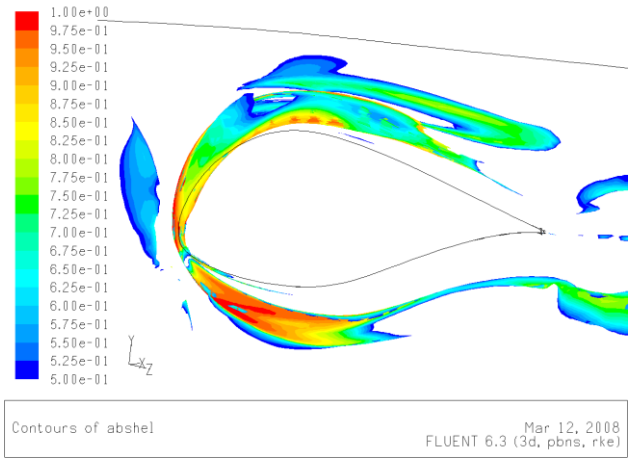

Fig. 18. Iso-surface of Q = 10 covered with contours of absolute helicity ranging from 0.5 to 1

Wind-tunnel visualizations, carried out for five angles of attack, confirmed the formation of a separation zone in the studied area as shown in Fig. 18.

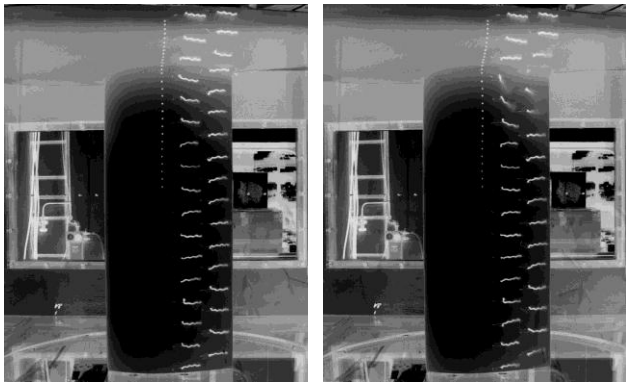

Fig. 18. Tuft visualization in CAT 865 x 485 x 900mm^3 wind tunnel test section on 1:5 scale model, $Re_c = 2 \cdot 10^5$, α = 5deg (left), α = 10deg (right). Long-exposure inverted photographs of the upper surface

Tuft visualization in the region of the TST10a wing-fuselage revealed a region of separated flow at V of 85 km/h IAS. A counter-rotating vortex generator of height h of 3mm was applied in chordwise location x/c of 0.48. Subsequent flight tests proved suppression of the separation (Fig. 19b).

Effect on the performance was established by measuring both the uncontrolled and controlled speed polar. Installation of the wing-root vortex generator VG resulted in a 5% L/D improvement for V = 85 km/h IAS. However, the positive influence is related only to the low-speed range. This result illustrates that change of the boundary layer properties, related to airspeed, have to be taken in account and the dimension of vortex generators has to be carefully optimised.

Fig. 19a. TST10a sailplane, wing root tuft visualization, V = 85 km/h IAS, uncontrolled case

Fig. 19b. TST10a sailplane, wing root tuft visualization, V = 85 km/h IAS, passive-flow control: vane-type VG, $x_{VGt}/c = 0.45$

Oil-flow visualization was carried out on HPH304S sailplane and another typical feature of wing-fuselage geometry flow was observed. Upwash in front of the wing and downwash behind the wing are influenced by additional fuselage crossflow velocity (alpha flow) at the junction. Due to induced angle of attack and usually divergent shape of the junction, the location of the boundary layer transition on the wing shifts upstream as we draw closer to the

junction forming a turbulent wedge. Systematic change of airfoils towards the wing root rib enabled large portion of laminar flow, Fig. 20. Turbulent wedge in typical position was not observed.

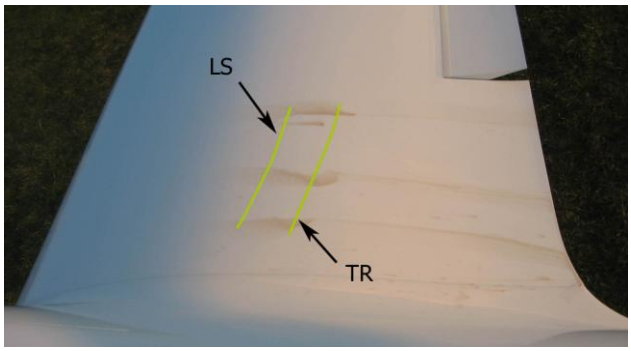

Fig. 20. HPH304S sailplane, wing root oil flow visualization, V = 100 km/h IAS, natural laminar separation (LS) and turbulent reattachment (TR)

6 Conclusions

Synthesis of CFD, wind-tunnel and in-flight experiments was used for analysis of nominally 2D and 3D boundary layers on sailplane geometries. Better insight into the flow physics was gained and several cases of flow control studied. Improvement of both performance and handling of examined sailplanes was reached.

7 Acknowledgment

The work has been supported by Ministry of Education, Youth and Sports of the Czech Republic within project No. 1M06031. Support by the Czech Science Foundation under grants No. IAA2076403 and No. GA 101/08/1112 is gratefully acknowledged.

Authors are indebted to their team colleagues, technicians and test pilots, namely Mr. Zdenek Kolek, Lubor Zeleny and Richard Jensen.

Thanks also belong to all Czech sailplane manufacturers, HPH Ltd., Mr. Jiri Hodan and Jaroslav Potmesil (HPH304S, 304C), TeST Ltd., Mr. Jan Friedl and Zdenek Teply (TST10) and finally SHVL Ltd., Mr. Pavel Tomana and Oto Vavrin (VSO10).

The support of Aeroclub Policka to continuing research is highly acknowledged.

8 References

[1] Thomas, F.: Fundamentals of Sailplane Design, 3rd Ed. College Park Press, 1999. 274 p. ISBN 0-9669553-0-7

[2] Althaus, D., and Wortmann, F.X., *Stuttgarter Profilkatalog I*, 1st ed., Vieweg & Sohn Verlagsgesellschaft, Braunschweig, 1981.

[3] Boermans, L.M.M. and Terleth, D.C.: Wind-tunnel Tests of Eight Sailplane Wing-Fuselage Combinations, *Technical Soaring*, Vol. 8, No. 3, 1984, pp. 70-85.

[4] Drela, M., Youngren, H.: Xfoil 6.9. MIT, 2001, 33 p., http://raphael.mit.edu/xfoil/

[5] Deperrois, A.: Analysis of foils and wings operating at low Reynolds numbers. Guidelines for XFLR5 V4.15, 2009, 53 p.

[6] Shih, T.-H., Liou, W. W., Shabbir, A., Yang, Z. and Zhu, J.: A New k-epsilon Eddy-Viscosity Model for High Reynolds Number Turbulent Flows - Model Development and Validation, *Computers Fluids*, 24(3):227-238, 1995

[7] Spalart P. and Allmaras, S.: A one-equation turbulence model for aerodynamic flows, Technical Report AIAA-92-0439, American Institute of Aeronautics and Astronautics, 1992

[8] Menter, F. R.: Two-Equation Eddy-Viscosity Turbulence Models for Engineering Applications, *AIAA Journal*, 32(8):1598-1605, August 1994

[9] Popelka, L.: Wind Tunnel Test Section for Aifoils and Bodies, Research Programme Feasibility Studies, *Proceedings of the Conference Topical Problems of Fluid Mechanics 2008*, Institute of Thermomechanics AS CR , Prague, 2008, pp. 85-88.

[10] Popelka, L.: Aerodynamic Optimization of Sailplane Airfoils, Ph.D. Dissertation, Department of Fluid Dynamics, Czech Technical University in Prague, 2006.

[11] Robinson, S. K.: Coherent Motions in the Turbulent Boundary Layer, *Annual Review of Fluid Mechanics*, Vol. 23., 1991, pp. 601-639.

Copyright Statement